ELSEVIER

Journal of Molecular Catalysis A: Chemical 109 (1996) 227–238

JOURNAL OF MOLECULAR CATALYSIS A: CHEMICAL

H_2 interaction with S atoms of a MoS_2 modelled catalytic site: electronic density analysis for S–H formation

Anibal Sierraalta, Fernando Ruette *

Laboratorio de Química Computacional, Centro de Química, Instituto Venezolano de Investigaciones Científicas, Apartado, 21827, Caracas 1020-A, Venezuela

Received 15 May 1995; accepted 23 January 1996

Abstract

Semi-core effective core potential (ECP2) calculations were carried out for Mo_3S_6 and Mo_2S_6 clusters that modelled MoS_2 catalyst surface sites (sulfur sites). The interaction of H_2 with monocoordinated (S_m) and bicoordinated (S_b) sulfur sites was studied. The topological properties of Mo–S bonds and the critical points (CP) of the charge density Laplacian ($-\nabla^2\rho(r_{cp})$), in the S valence shell, were analyzed. The results indicate that H_2 is dissociated over sites formed by two neighbor S atoms. The local interaction of H_2 with the S atoms occurs in the region in which there is the highest spin density concentration; i.e., the zone located at the CP maxima of $-\nabla^2\rho_{spin}(r_{cp})$. This work shows the importance of calculating the CP of $-\nabla^2\rho(r_{cp})$ on the surface atoms to determinate active sites on a surface.

Keywords: H_2 dissociation; Effective core potential (ECP); Electronic density topology; Bader's theory; Molybdenum sulphide

1. Introduction

Hydrodesulfurization (HDS) or the removal of sulfur from sulfur-containing molecules (C_xH_yS) is a crucial step in the refinement process of heavy oils. The HDS reaction, at the industrial level, is performed over heterogeneous catalysts of molybdenum disulfide (MoS_2) anchored over a nonreactive support. The overall chemical reaction takes place in the presence of hydrogen:

$$C_xH_yS + nH_2 \xrightarrow[\Delta]{\text{catalyst}} \text{hydrocarbons} + H_2S$$

Before the MoS_2 can be used as a catalyst, it must be pretreated with H_2 or H_2/H_2S at high temperatures. During this process the H_2, in a first step, is dissociated forming –SH groups over the MoS_2 surface that later evolves H_2S, leading to the formation of vacancies on the metallic atoms. It has been shown in the literature [1–4], that these groups (–SH) and the vacancies on the metallic atom are essential in the HDS catalytic activity. It is very important then, to understand how and where these –SH groups are formed in order to model new materials or new catalysts for HDS processes.

In spite of its technological importance, few theoretical studies in this field have been performed. Anderson [5], using a semiempirical method studied the hydrogen adsorption on MoS_2. Pis Diez and Jubert [6,7], using extended

* Corresponding author.

PII S1381-1169(96)00036-2

Hückel, found that the hydrogen absorption is more favored over the Mo atoms than over the S atoms, and that the corner sites are the most active sites for adsorption of one or two H atoms, but no molecular hydrogen adsorption was considered. The molecular dissociation of H_2 over small nickel sulfide cluster was studied by Neurock and Van Santen [8] using the local spin density approximation. They showed that the H_2 molecules dissociate heterolytically forming sulfhydryl (SH) and hydryl (NiH) species.

As has been shown in the literature, the topology of the molecular electronic density, $\rho(\boldsymbol{r})$, can be used to characterize both the atomic interaction in molecules and the reactivity [9–12]. The theory *Atoms in Molecules* [12] (AIM) has the advantage that it is independent of any orbital formalism. Molecular properties definitions based on atomic orbital population (Mulliken, Löwdin, etc) in many cases lack physical significance [13]. For example, in MoS_4^{2-} [14], the Mo is negative according to Mulliken population, but using Bader's topological analysis [12] the charge on the metal is positive. The AIM theory deals with the total electronic density which is a molecular property that can be determined experimentally by means of X-ray diffraction.

The reactivity of a molecular system can be mirrored by the critical points (CP) of the negative of the Laplacian of $\rho(\boldsymbol{r})$ $(-\nabla^2\rho(\boldsymbol{r}))$. This quantity reveals where the electronic density is locally concentrated or depleted in a molecular system and these local electronic charge concentrations and depletions can be related to the Lewis acid–base model.

To the best of our knowledge, no topological analysis of the electronic charge distribution of the active sites of MoS_2 has been done. Even more, this is the first application in which the ab initio effective core potential method (ECP) has been used to characterize the topological properties of ρ and $\nabla^2\rho$ in catalytic systems. In this work, we have applied Bader's theory to study the H_2 interaction with S atoms on a MoS_2 modelled surface (Mo_3S_6 and Mo_2S_6 clusters). The magnitude of the electronic density (ρ_{crit}), the Laplacian ($\nabla^2\rho_{crit}$), the ellipticity (ϵ), the ratio of the curvatures $|\lambda_1/\lambda_3|$ and the kinetic energy per electron G_{crit}/ρ_{cri} at the bond critical points (BCP) are discussed. In addition, an analysis of the maxima of $-\nabla^2\rho(\boldsymbol{r})$ and the spin density for each cluster is performed. Relief maps of $-\nabla^2\rho(\boldsymbol{r})$ are displayed, as well as a schematic representation of the location of each corresponding maximum. In order to investigate the possibility of a direct S–S bond, the Mo_2S_6 cluster was relaxed conserving the symmetry clusters.

2. Theoretical background

The characterization of chemical bonds in a molecular system can be derived from the topological properties of $\rho(\boldsymbol{r})$, as has been established by Bader et al. [12]. The Laplacian $(-\nabla^2\rho(\boldsymbol{r}))$ has become a useful tool in the interpretation of quantum chemical results, because it provides an enhanced view of the local form of the electronic density. Thus, regions where $-\nabla^2\rho(\boldsymbol{r}) > 0$ correspond to zones where electronic charge is concentrated and vice versa (regions $-\nabla^2\rho(\boldsymbol{r}) < 0$ correspond to zones where electronic charge is depleted). The topological study of $-\nabla^2\rho(\boldsymbol{r})$ in the valence shell region permits the determination of the number and the location of electron pairs proposed in the Lewis and VSEPR or VSEPD [12,15–18] models. In some respects, this quantity mimics the equivalent spatial properties of localized molecular orbitals.

Critical points (CP) of a function $F(\boldsymbol{r})$ (where F may be $\rho(\boldsymbol{r})$ or $-\nabla^2\rho(\boldsymbol{r})$) are those where $\nabla F = 0$ and are characterized by the eigenvalues (λ_i $i = 1, 2, 3$) of the Hessian matrix of F (the curvatures of F) at each CP. These points are classified in accord with the rank (σ) (number of non-zero eigenvalues of the Hessian matrix), and to the signature (s) (the difference between the number of positive and negative eigenval-

ues). That is, each CP is then labeled as (σ, s). Thus, $(3,-1)$ and $(3,+1)$ CP's (two curvatures with the same sign) correspond to saddle points; $(3,-3)$ to local maxima; and $(3,+3)$ to local minima.

Using the above nomenclature for the CP's and the values of λ_i's, one can classify the atomic interactions or bonds. The $\nabla^2\rho(\boldsymbol{r})$ value at CP is given by: $\nabla^2\rho(\boldsymbol{r}_{\mathbf{CP}}) = \lambda_1 + \lambda_2 + \lambda_3$. For example, a $(3,-1)$ CP (λ_1, $\lambda_2 < 0$ and $\lambda_3 > 0$) represents a local maximum in two directions and a local minimum in the third one. If the CP is located in the internuclear line, the negative curvatures (λ_1 and λ_2) of $\rho(\boldsymbol{r})$ at the CP indicate the degree of charge density contraction in a region perpendicular to the interatomic interaction line. On the other hand, the magnitude of positive curvature measures the degree of charge depletion toward the nuclei. In general, $|\lambda_1|/\lambda_3 > 1$ implies charge concentration on the interatomic region; i.e., shared interactions (covalent bond). Contrarily, if $|\lambda_1|/\lambda_3 < 1$, it means that charge depletion occurs in the internuclear line; i.e., closed-shell interactions (ionic bonds).

Another way to assess the interatomic interaction (closed-shell or shared) is by the kinetic energy per unit charge ($G_{\mathrm{crit}}/\rho_{\mathrm{crit}}$) at the CP, defined in terms of the orbital density gradients ($\nabla\rho_i$) and the occupation numbers (n_i) as:.

$$G_{\mathrm{crit}} = \left(h/2\pi^2 m\right) \sum_i n_i \nabla\rho_i \cdot \nabla\rho_i/\rho_i$$

If $G_{\mathrm{crit}}/\rho_{\mathrm{crit}} < 1$ the bond has covalent character and if $G_{\mathrm{crit}}/\rho_{\mathrm{crit}} > 1$ the interaction are of ionic nature [9].

The accumulation of charge in a particular plane may be used for characterizing the type of bond (π or σ character) in accord with its symmetry. This property can be measured with the ellipticity (ϵ) defined as $\epsilon = (|\lambda_1|/\lambda_2 - 1)$, where $|\lambda_1| > |\lambda_2|$.

The local $(3,-3)$ and $(3,+1)$ critical points of $-\nabla^2\rho(\boldsymbol{r})$ at the valence shell charge concentration (VSCC) of an atom in a molecule can be used to analyze the physical basis of the Lewis acid–base reaction model [12,18]. The regions of local charge concentration in the Lewis base react with the regions of local charge depletion of a Lewis acid. In general, the basicity or acidity and the molecular structures could be explained in terms of the topology of $-\nabla^2\rho(\boldsymbol{r})$. For example, MacDougall et al. [19] have proposed that the most stable molecular geometry of $VOCl_3$ corresponds to the largest separation of local maxima in the VSCC of the V atom, defined by the $(3,-3)$ critical points of $-\nabla^2\rho(\boldsymbol{r})$.

The topological properties of $\rho(\boldsymbol{r})$ for some molybdenum compounds, at the Mo–X bonds (X = S, O, Cl) were studied in a previous paper [14], using different ECP approaches (ECP2 and ECP1) and the full-electron HF method. The best results were obtained when the effective core potential includes the outermost core electrons (ECP2); i.e., when the $4s^2$, $4p^6$, $4d^5$ and $5s^1$ are used, as active electrons for the Mo atom. The ECP1 approach, which only uses the $4d^5$ and $5s^1$ electrons, fails in the description of the bond critical points. Similar results were found by Frenking et al. [20,21], using Ti and Fe compounds.

3. Methodology and modelled surface active sites

Semi-core effective core potential–UHF calculations were performed for Mo_3S_6, Mo_2S_6, $Mo_3S_6H_2$ and $Mo_2S_6H_2$ clusters, using the HONDO-8 program from the MOTECC-90 package [22]. The clusters Mo_3S_6 and Mo_2S_6, shown in Fig. 1, were employed in order to simulate the monocoordinate sulfur atoms type (S_m) and the bicoordinate ones (S_b) in a MoS_2 surface. The interatomic distances were taken from the crystal structure of molybdenite [23].

According to the literature, the active sites for the HDS reaction are located at the edge of small MoS_2 crystallites. Wambeke et al. [3](a) suggest that at the first stage of the activation of the MoS_2/γ-Al_2O_3 catalyst, the monocoordi-

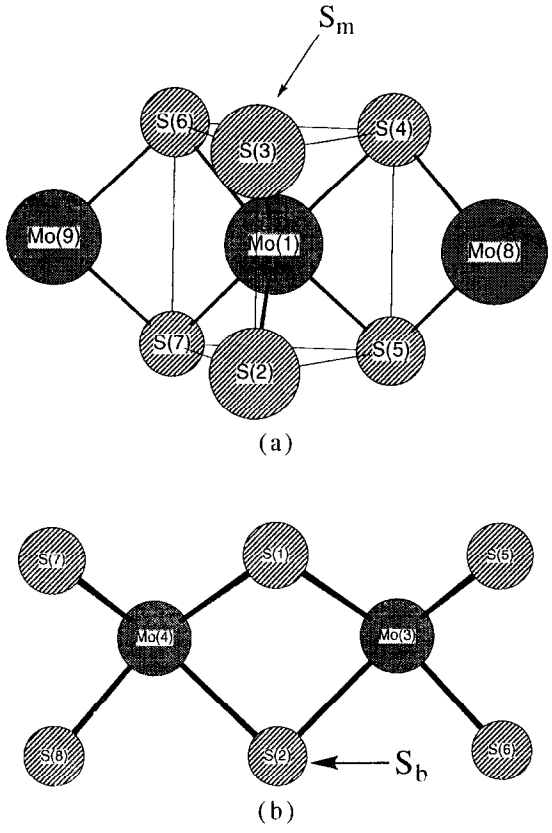

Fig. 1. Clusters used to model S_m and S_b sites on a MoS_2 surface. (a) Mo_3S_6. (b) Mo_2S_6.

nate sulfurs (S_m) at the surface have been eliminated, leading to Mo sites without S atoms. Diemann et al. [4] propose that strongly unsaturated active sites appear on the edges of MoS_2-like crystallites. The Mo_3S_6 and Mo_2S_6 clusters were chosen to mimic the sulfur sites at the edge of small crystallites. These clusters present S–S bonds, see below, as proposed by Diemann et al. [4] and Rakowski DuBois and others [24], giving an oxidation number for the central Mo atom between 3 and 6, depending on the formation of $(S_2)^{2-}$ groups.

The ECP used for S, and H atoms was that proposed by Stevens et al. [25]. The LaJohn et al. [26] semi-core ECP was employed for the Mo atom with modifications in the atomic basis set [14], i.e., the 5*s*-function was replaced by a split *d*-function. The critical points of $-\nabla^2\rho(\boldsymbol{r})$ were calculated with a locally modified version of the EXTREM program [27] and Bader's electronic charges with the PROAIM program [28].

4. Results and discussion

4.1. Bonding properties of Mo–S bonds

Numerical calculations of the topological properties of the Mo–S bond (the (3, − 1) CPs located on the interatomic line) for the Mo_3S_6 and Mo_2S_6 clusters (see Fig. 1), and MoS_4^{2-} were performed. The values of the Mo–CP distance (R_{Mo-CP}), density at the CP (ρ_{crit}),

Table 1
Topological properties of the Mo–S bond critical point in Mo_3S_6, Mo_2S_6 clusters and MoS_4^{2-} molecule [a]

Bond	Mo–S [e]	Mo–S_b		Mo–S_m
Cluster	MoS_4^{2-}	Mo_2S_6 (unrelax.)	Mo_2S_6 (relax.)	Mo_3S_6
R_{Mo-CP} [b] (Å)	1.14 (2.21)	1.18 (2.41)	1.30 (2.65)	1.17 (2.41)
ρ_{crit}	0.113	0.065	0.051	0.074
$-\nabla^2\rho_{crit}$	−0.137	0.201	0.072	0.171
ϵ	0.000	0.129	0.013	0.116
$\lvert\lambda_1/\lambda_3\rvert$	0.316	0.174	0.265	0.219
G_{crit}/ρ_{crit}	0.678	0.973	0.574	0.810
Net charge [c]	−0.88	−0.51	−0.67	−0.35
$\lvert N\alpha - N\beta\rvert$ [d]	0.00	1.01	1.08	1.35

[a] All values in atomic units.
[b] Distance from Mo atom to the bond critical point. The values in parentheses correspond to Mo–S distance.
[c] On S atom.
[d] Net spin population on S atoms.
[e] From ref. [14](a).

density Laplacian ($-\nabla^2\rho_{crit}$) ellipticity (ϵ), $|\lambda_1/\lambda_3|$, G_{crit}/ρ_{crit}, net charge, and the net spin population ($|N\alpha - N\beta|$) are shown in Table 1. The geometrically relaxed Mo_2S_6 cluster maintaining the symmetry was also considered, in order to see how the topological properties of the total electronic density are affected by the optimization of the geometry.

According to the values of $-\nabla^2\rho_{crit} < 0$ (small values), $|\lambda_1/\lambda_3| < 1$, and low value of ρ_{crit}, the Mo–S bond can be classified as a closed-shell interaction (a depletion of charge from the bond); nevertheless, the value of $G_{crit}/\rho_{crit} < 1$ indicates a shared interaction. These results suggest that the Mo–S bond can be classified as an intermediate type.

The distance from the Mo atom to the (3,− 1) CP (R_{Mo-CP}) in the Mo–S bond is, as expected, depending on the Mo–S distance (see values in parentheses). Similar R_{Mo-CP} distances was found for clusters and MoS_4^{2-}, except for the relaxed Mo_2S_6 cluster, where the R_{Mo-CP} is longer, due to the enlargement of the Mo–S distance.

The net spin population ($|N\alpha - N\beta|$) shows that both types of S atoms (S_m and S_b) have a large unpaired electronic population. The ellipticities (ϵ) reveal that there is a π contribution to the Mo–S bond that is absent in the MoS_4^{2-} molecule.

In the unrelaxed Mo_2S_6 cluster, besides the (3,− 1) Mo–S CP's, there is a (3,+ 1) CP that is characteristic of ring bonded atoms [12]. This CP is localized in the middle of the ring formed by the atoms S(1)–Mo(3)–S(2)–Mo(4) (see Fig. 1b). For the relaxed structure, this (3,+ 1) CP does not exist but a (3,− 1) CP appears between the S_b atoms (S(1) and S(2)). This is an indication of the formation of a S_b–S_b bond which is slightly curved toward the midpoint Mo–Mo line. It has the following characteristics: an angle S_b–CP–S_b of 170.8 degrees, a low ρ_{crit} value ($\rho_{crit} = 0.021$ au), $-\nabla^2\rho_{crit} = 0.048$ au, $G_{crit}/\rho_{crit} = 0.621$ au and a high ellipticity (ϵ = 11.455). The changes in the ellipticities of Mo − S_b bonds between the unrelaxed and relaxed Mo_2S_6 clusters is due to a strong π contribution that comes from the participation of the p orbitals of the S atom in the S–S bond. Therefore, in Mo_2S_6, the Mo–S_b bonds increase their σ-character, diminishing the ϵ value with respect to the unrelaxed cluster, see Table 1.

Table 1 also shows that the S_b atoms have a greater net charge than the monocoordinated S atoms (S_m), contrary to the net spin population ($|N\alpha - N\beta|$). Considering this result and the existence of a CP between the S_b atoms, we may conclude that in the relaxed structure of the Mo_2S_6 cluster, the bridged sulfur atoms (S_b) are forming a $(S_2)^{n-}$ group (n between 1 and 2) with two uncoupled electrons. This result is in agreement with findings of Raman spectroscopy reported by Knözinger et al. [29]. They have shown that the $(S_2)^{2-}$ group could be present in the MoS_2 surfaces. Similar results are presented in the review of Rakowski DuBois [24](a) for $Mo_2S_4(Cp)_2$, complexes and in Müller's survey [24](b) for Mo–S compounds. According to our results and experimental evidences, the $(S_2)^{2-}$ group could exist in the MoS_2 clusters, having a bridge-like geometry. No Mo–Mo bond critical point was found for Mo_2S_6 and Mo_3S_6 clusters, suggesting that the Mo atoms in very small clusters are joined by means of sulfur bridges.

4.2. $-\nabla^2\rho(r)$ topology at the sulfur valence shell

The critical points of $-\nabla^2\rho(r)$ at the valence region give information where the valence electronic charge is highly concentrated or depleted [9–12]. Therefore, as mentioned above, in a molecular structure the number and the characteristics of the critical points of $-\nabla^2\rho(r)$ are strongly correlated with the number and the nature of the atoms that interact. In this sense, the active sites can be mirrored by the $-\nabla^2\rho(r)$ topology.

In Fig. 2, a relief map of the $-\nabla^2\rho(r)$ of the Mo_3S_6 cluster is shown. The values of $-\nabla^2\rho(r)$ were projected in the plane that cuts the middle of the S_m atoms (S(2) and S(3)) and the central

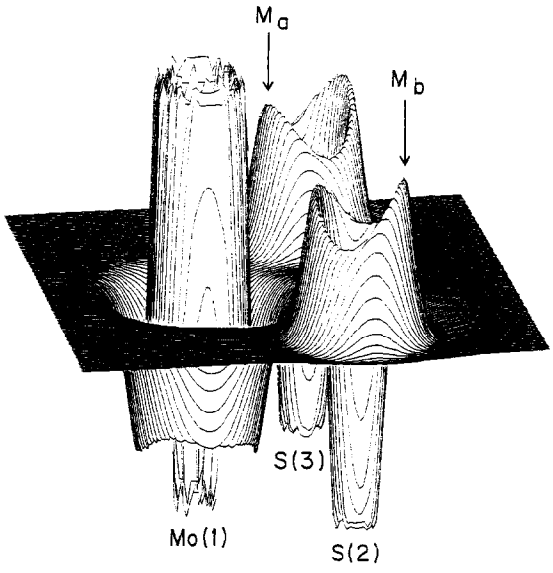

Fig. 2. Relief map of $-\nabla^2\rho(r)$ for Mo_3S_6 cluster in the plane where the (3,−3) critical points of the S(2) and S(3) valence shell lie. See Fig. 1a.

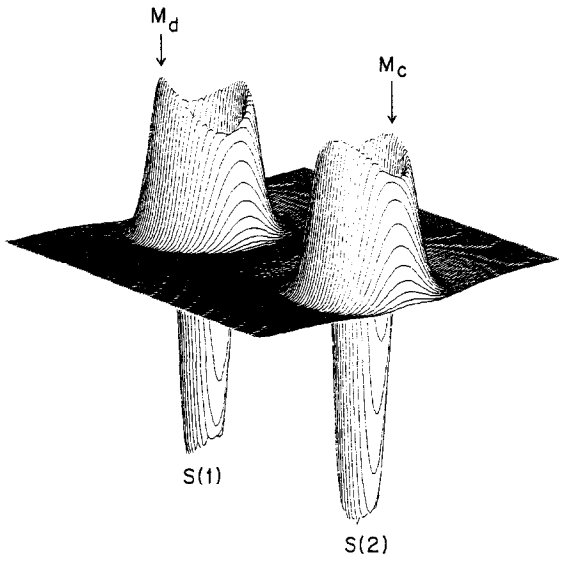

Fig. 3. Relief map of $-\nabla^2\rho(r)$ for Mo_2S_6 cluster in the plane where the (3,−3) critical points of the S(1) and S(2) valence shell lie. See Fig. 1b.

Mo atom (Mo(1)). The $-\nabla^2\rho(r)$ of S_m valence shell shows two maxima that correspond to (3,−3) CP's. One lies in the Mo–S_m bond region, facing the Mo atom ($\mathbf{M_a}$) and the other lies in the opposite direction ($\mathbf{M_b}$).

Fig. 3 displays a relief map of the $-\nabla^2\rho(r)$, for the Mo_2S_6 unrelaxed cluster in the plane where the (3,−3) critical points of the S_b valence shell lie. This plane cuts the S(1) and S(2) atoms and is perpendicular to the Mo(3)–Mo(4) line. The topology of $-\nabla^2\rho(r)$ for the S_b atoms is similar to that found for S_m ones, i.e., both maxima lie in a plane that contains two S_b atoms and are perpendicular to the plane formed by Mo atoms. The $-\nabla^2\rho(r)$ valence shell shows two (3,−3) CP's: one faces inside the cluster ($\mathbf{M_c}$) and the other faces in the opposite direction ($\mathbf{M_d}$).

The values of $-\nabla^2\rho(r)$ and $\rho(r)$ at the (3,−3) CP's of the sulfur valence shell, and distances (D) between CP's of the same type are presented in Table 2. The CP's ($\mathbf{M_a}$, $\mathbf{M_c}$ and $\mathbf{M_{c'}}$) that face toward the Mo atom or those that face inside (FI) the MoS_2 clusters present a lower electronic charge concentration than the CP's ($\mathbf{M_b}$, $\mathbf{M_d}$ and $\mathbf{M_{d'}}$) that face outside (FO) the cluster. Note that $\mathbf{M_{c'}}$ and $\mathbf{M_{d'}}$ correspond to the relaxed cluster. The sulfur atom S_b possesses a greater local charge concentration at the

Table 2
Values of $-\nabla^2\rho(r)$ and $\rho(r)$ at the S valence shell (3,−3) CP and the distance (D) between two near $\mathbf{M_i}$ (i = a, b, c, d, c', d') CP for Mo_3S_6 and Mo_2S_6 clusters [a]

Cluster	Critical point	(3,−3) FI CP [b]			Critical point	(3,−3) FO CP [c]		
		$-\nabla^2\rho(r)$	$\rho(r)$	D		$-\nabla^2\rho(r)$	$\rho(r)$	D
Mo_3S_6	$\mathbf{M_a}$	0.844	0.182	4.299	$\mathbf{M_b}$	0.936	0.187	7.550
Mo_2S_6 (unrelax.)	$\mathbf{M_c}$	0.877	0.186	4.824	$\mathbf{M_d}$	0.969	0.193	7.123
Mo_2S_6 (relax.)	$\mathbf{M_{c'}}$	0.888	0.182	5.711	$\mathbf{M_{d'}}$	0.991	0.193	6.820

[a] All values in atomic units.
[b] FI means that the CP faces inside the cluster.
[c] FO means that the CP faces outside the cluster.

valence shell than the S_m atom. These results, together with Bader's net charge (see Table 1), show that the S_b sulfur type are more basic than the S_m ones and therefore more susceptible of an electrophilic attack.

The relaxation of the Mo_2S_6 cluster slightly increases the local charge concentration in the FO CP's, but reduces the distance between two of them (from 7.123 to 6.820 au) and increases the separation between two near FI CP's (from 4.824 to 5.711 au). Because the distances between FO and between FI CP's are enlarged and shortened, respectively, when the system is relaxed, the distance between FI and FO CP's in a S atom is enlarged. This fact is in agreement with MacDougall's work [19] in which the author suggests that the minimum energy geometry is one that maximizes the separation between local concentrations of charges.

As been stated above, in the MoS_2 clusters each sulfur atom possesses an unpaired electron. The presence of this electron would not be detected in the plot of $-\nabla^2\rho(\boldsymbol{r})$ or $\rho(\boldsymbol{r})$ due to the effect of the other electrons to mask the small outcome from one electron in the total valence electron density distribution. On the other hand, this unpaired electron is usually associated with the highest occupied molecular orbitals (HOMOs), and therefore it is a reactive electronic charge density. In order to find out where this unpaired electron density is locally concentrated or depleted, the topology of the total spin density Laplacian ($-\nabla^2\rho_{spin}(\boldsymbol{r})$) was analyzed. Here, $\rho_{spin}(\boldsymbol{r})$ is defined as $\rho_\alpha(\boldsymbol{r}) - \rho_\beta(\boldsymbol{r})$, where $\rho_\alpha(\boldsymbol{r})$ and $\rho_\beta(\boldsymbol{r})$ are the total electronic density for α and β electrons, respectively.

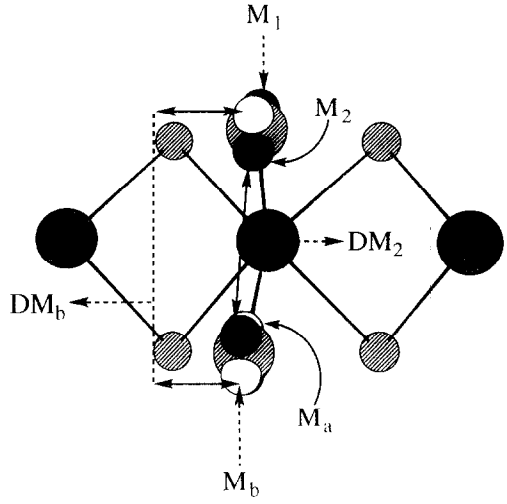

Fig. 4. Schematic representation of the spatial positions of maxima of $-\nabla^2\rho(\boldsymbol{r})$ and $-\nabla^2\rho_{spin}(\boldsymbol{r})$ for Mo_3S_6 cluster. The white half-spheres correspond to $-\nabla^2\rho(\boldsymbol{r})$ maxima. The black half-spheres correspond to $-\nabla^2\rho_{spin}(\boldsymbol{r})$ maxima. The dashed spheres are assigned to S and the gray ones to Mo atoms.

A schematic representation of the position of maxima of $-\nabla^2\rho(\boldsymbol{r})$ and $-\nabla^2\rho_{spin}(\boldsymbol{r})$ for the Mo_3S_6 cluster is given in Fig. 4. As can be noted, the maxima of $-\nabla^2\rho_{spin}(\boldsymbol{r})$ ($\mathbf{M_1}$ and $\mathbf{M_2}$ CP's) are in the same plane as the maxima of $-\nabla^2\rho(\boldsymbol{r})$ ($\mathbf{M_a}$ and $\mathbf{M_b}$ CP's), but they are in a perpendicular direction to the latter. In the case of Mo_2S_6 clusters a similar pattern was obtained (see Fig. 5). The maxima of $-\nabla^2\rho_{spin}(\boldsymbol{r})$ ($\mathbf{M_3}$ and $\mathbf{M_4}$ CP's) are in the same plane and

Table 3
Values of $-\nabla^2\rho_{spin}(\boldsymbol{r})$ and $\rho_{spin}(\boldsymbol{r})$ at the S valence shell (3, − 3) CP and the distance (D) between two near $\mathbf{M_i}$ (i = 1, 2, 3, 4, 3′, 4′) CP for Mo_3S_6 and Mo_2S_6 clusters [a]

Cluster	Critical point	(3, − 3) FI CP [b]			Critical point	(3, − 3) FO CP [c]		
		$-\nabla^2\rho_{spin}$	ρ_{spin}	D		$-\nabla^2\rho_{spin}$	ρ_{spin}	D
Mo_3S_6	$\mathbf{M_1}$	0.471	0.073	7.527	$\mathbf{M_2}$	0.406	0.065	4.367
Mo_2S_6 (unrelax.)	$\mathbf{M_3}$	0.338	0.052	7.865	$\mathbf{M_4}$	0.351	0.051	4.151
Mo_2S_6 (relax.)	$\mathbf{M_{3'}}$	0.303	0.048	8.245	$\mathbf{M_{4'}}$	0.327	0.050	4.135

[a] All values in atomic units.
[b] FI means that the CP faces inside the cluster.
[c] FO means that the CP faces outside the cluster.

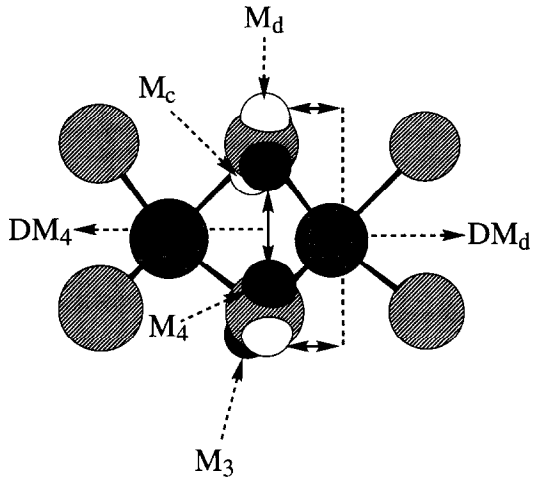

Fig. 5. Schematic representation of the spatial positions of the maxima of $-\nabla^2\rho(r)$ and $-\nabla^2\rho_{spin}(r)$ for Mo_2S_6 cluster. The white half-spheres correspond to $-\nabla^2\rho(r)$ maxima. The black half-spheres correspond to $-\nabla^2\rho_{spin}(r)$ maximum. The dashed spheres are assigned to S and the gray ones to Mo atoms.

are perpendicular to the maxima of $-\nabla^2\rho(r)$ ($\mathbf{M_c}$ and $\mathbf{M_d}$ points).

The values of $-\nabla^2\rho_{spin}(r)$, $\rho_{spin}(r)$ at the (3,−3) CP's of the valence shell and the distance between nearest maxima (D) are listed in Table 3. As expected, the values of ρ_{spin} are lower than the values of ρ, because ρ_{spin} is related with a total charge of about 1 electron, instead of 6 or more electrons of the S valence shell. The unrelaxed and relaxed Mo_2S_6 clusters have similar values of ρ_{spin} for the FO CP's, as well as for the FI cases. However, Mo_2S_6 $-\nabla^2\rho_{spin}(r)$ and $\rho_{spin}(r)$ present lower values than those of the Mo_3S_6 cluster.

4.3. Interaction of MoS_2 with H_2

In order to study the H_2 dissociation process on the S atoms, calculations were carried out by approaching the H_2 molecule to a S_m or a S_b atom of Mo_3S_6 and Mo_2S_6 clusters (three-center mechanism) in the direction of the maxima of $-\nabla^2\rho(r)$ ($\mathbf{M_b}$ or $\mathbf{M_d}$ CP shown Figs. 4 and 5). In the three-center mechanism, the S atom, the $\mathbf{M_b}$ or $\mathbf{M_d}$ point, and the H_2 midpoint bond, lie in a straight line. Although the H_2 molecule is free to rotate around this straight line, only two geometrical conformations were studied. The H_2 bond line was placed parallel or perpendicular to an imaginary line that joins the Mo atoms. For this path, it was not possible to obtain H_2 dissociation, probably due to a high electronic repulsion between the local charge concentration of the S atom and the H_2 electrons. Nevertheless, in order to describe correctly the breaking of one H–H bond and formation of two S–H bonds it is necessary to include the part of the electronic correlation that is absent at the HF level. This results indicate that the dissociation of H_2 over one sulfur atom (S_b or S_m) does not seem to occur, because the electronic density associated with the $\mathbf{M_b}$ and $\mathbf{M_d}$ points is strongly bonded to the S atom, and therefore, is not reactive.

Because these calculations were carried out at UHF level, the topological properties of the spin density Laplacian ($-\nabla^2\rho_{spin}(r)$) ($\rho_{spin}(r) = \rho_\alpha(r) - \rho_\beta(r)$ is the difference between alpha and beta electron densities) were also considered. The maxima of $-\nabla^2\rho_{spin}(r)$ correspond to spatial localization of spin concentrations that may be associated with unpaired electrons that occupied some molecular orbitals, mainly localized on S atoms. The fact that there are unpaired electrons on S atoms agrees with the simple Lewis picture of unpaired electrons in the S_m atoms of Mo_3S_6 and with the formation of unpaired electrons in S_b atoms, due to the formation of $(S_2)^{2-}$ groups in the Mo_2S_6 cluster. The reactivity of $(S_2)^{2-}$ groups has been experimentally reported by Rakowski DuBois [24](a) for the chemisorption of alkynes and hydrocarbon reactions with H_2. The experimental results for ethylene and acetylene have been explained in theoretical work by Yu and Anderson [30] in terms of frontier orbitals.

Due to the above mentioned results, it seems that the best dissociation path involves two FO $-\nabla^2\rho_{spin}(r)$ maxima that belong to two S_m or S_b atoms ($\mathbf{M_2}$ or $\mathbf{M_4}$ CP; see Figs. 4 and 5). This path leads to a four-center mechanism. Our calculations show that when H_2 is approxi-

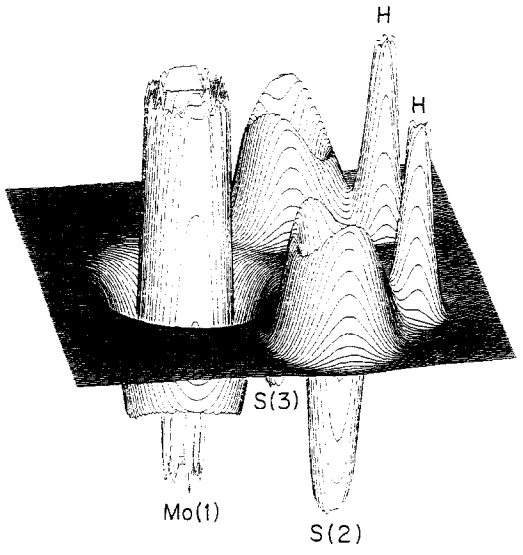

Fig. 6. Relief map of $-\nabla^2\rho(\boldsymbol{r})$ for $Mo_3S_6H_2$ cluster in the plane of S(2), S(3), Mo(1) and H atoms, showing the (3,−1) critical points of the S–H bond.

mated in the direction of the two FO $-\nabla^2\rho_{spin}(\boldsymbol{r})$ maxima, it dissociates, producing two –SH groups. A relief map of $-\nabla^2\rho(\boldsymbol{r})$ in the plane of the S(2), S(3), Mo(1) and H atoms is presented in Fig. 6. It is observed that there is no charge density in the region between the H atoms and an important charge density in the internuclear lines of the S–H bonds (saddle points (3,− 1)).

These results may be explained in terms of unpaired electrons of frontier orbitals located on S atoms (S_m or S_b). The highest occupied molecular orbitals (HOMO's) of open-shell systems correspond to unpaired electrons. These electrons in the S atoms are able to interact stronger than in the case of two closed-shell interactions (interaction of H_2 with $\mathbf{M_b}$ or $\mathbf{M_d}$ CP of S), because in the former the electron–electron repulsion is smaller (compare $\rho_{spin}(\boldsymbol{r})$ with $\rho(\boldsymbol{r})$ in Tables 3 and 2, respectively). In addition, because the S atoms are negatively charged, the frontier orbitals are less stable; therefore, an electronic charge transfer between S atoms and the H_2 antibonding σ^* orbital may occur, facilitating in this way the H_2 dissociation.

It is good to note at this point that the location and orientation of the spin density CP maxima may be associated with the location and orientation of the active site in the sulfur atoms. Therefore, the fact of determining the position of spin concentration densities on surface atoms may facilitate the localization of optimal places for chemisorption and dissociation of the H_2 molecule on the surface. This feature is very important, because it helps to save much time in ab initio calculations. Thus, only one single calculation, that does not include the adsorbate, is sufficient to determine the adsorbate–cluster interaction sites, which, in standard quantum chemistry methodologies, require a large and tedious optimization procedure.

Table 4 displays the topological properties of the S–H bond in the $Mo_3S_6(H_2)$ and $Mo_2S_6(H_2)$ clusters, as well as for H_2S. For all cases the S–H cluster bond is quite similar to the S–H bond in the H_2S molecule, showing that this bond is completely formed. The S–H

Table 4
Topological properties of the S–H bond critical point in $Mo_3S_6(H)_2$, $Mo_2S_6(H)_2$ clusters and H_2S molecule [a]

Bond	S_m–H	S_b–H		S–H
Cluster	$Mo_3S_6(H)_2$	$Mo_2S_6(H)_2$ (unrelax.)	$Mo_2S_6(H)_2$ (relax.)	H_2S
R_{S-CP} [b] (Å)	0.84 (1.38)	0.81 (1.36)	0.80 (1.35)	0.81 (1.36)
ρ_{crit}	0.165	0.169	0.170	0.171
$-\nabla^2\rho_{crit}$	0.311	0.350	0.358	0.369
$\lvert\lambda_1/\lambda_3\rvert$	1.396	2.230	2.241	2.297
G_{crit}/ρ_{crit}	0.245	0.274	0.289	0.266

[a] All values in atomic units.
[b] Distance from S atom to the bond critical point. The values in parentheses correspond to S–H distance

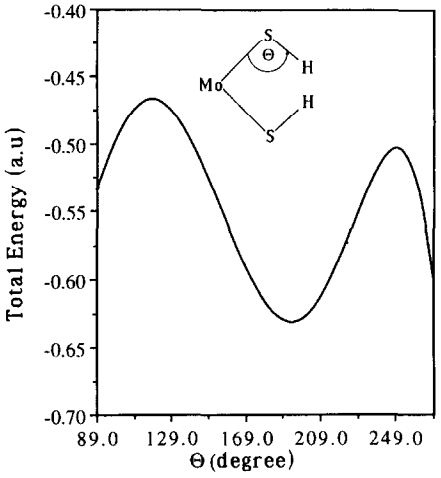

Fig. 7. Potential energy curve for the opening of the Mo–S–H angle.

bond has covalent characteristics: $-\nabla^2\rho(r) > 0$, $|\lambda_1/\lambda_3| > 1$, and $G_{crit}/\rho_{crit} < 1$.

Table 5 shows the topological properties of the Mo–SH bond in $Mo_3S_6(H_2)$ and $Mo_2S_6(H_2)$ clusters. In comparison to the values of Table 1, there are no large changes, except a decrease in the ρ_{crit} values, showing that a weakening of the Mo–S bond occurs after formation of the S–H group. The ϵ values ($\epsilon = (|\lambda_1|/\lambda_2 - 1)$, increase as a consequence of the S–H bond formation. The two curvatures λ_1 and λ_2 are less equal, because the curvature in the plane H–S–Mo–S is varied by the change in the *s–p* hybridization caused by the formation of the S–H bond.

Table 5
Topological properties of the Mo–SH bond critical point in $Mo_3S_6(H)_2$, $Mo_2S_6(H)_2$ clusters [a]

Bond	Mo–(S_mH)	Mo–(S_bH)	
Cluster	Mo_3S_6	Mo_2S_6 (unrelax.)	Mo_2S_6 (relax.)
R_{Mo-CP} [b] (Å)	1.26 (2.41)	1.17 (2.41)	1.27 (2.65)
ρ_{crit}	0.049	0.048	0.048
$-\nabla^2\rho_{crit}$	−0.145	0.192	0.111
ϵ	0.159	0.150	0.173
$\lvert\lambda_1/\lambda_3\rvert$	0.194	0.204	0.218
G_{crit}/ρ_{crit}	0.914	0.894	0.763

[a] All values in atomic units.
[b] Distance from Mo atom to the bond critical point. The values in parentheses correspond to Mo–SH distance

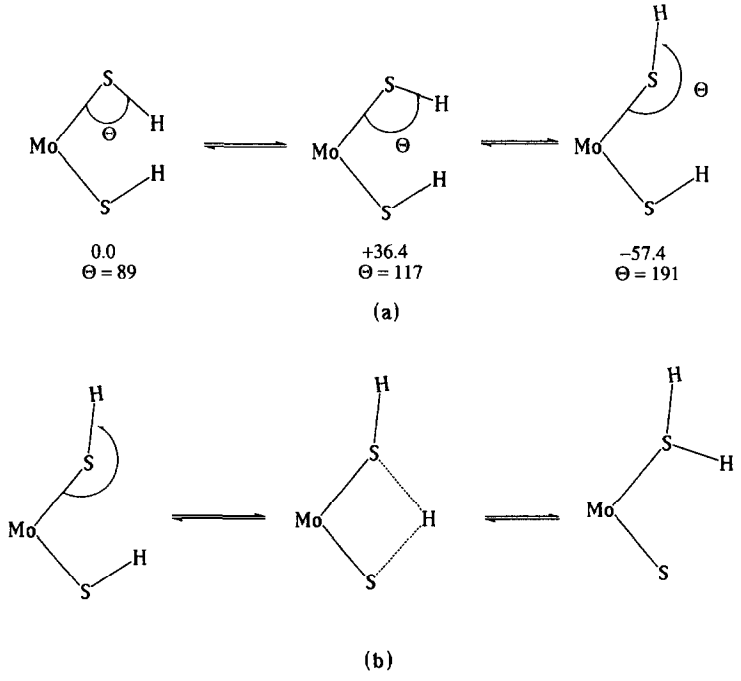

Fig. 8. (a) Energy difference (kcal/mol) and the Mo–S–H angles (Θ) for the initial, the highest and the lowest conformations in the $Mo_3S_6H_2$ system. (b) A possible mechanism of H_2S formation by H transfer in a MoS_2 surface.

In order to gain insight into the possible mechanism of the H_2S formation, the opening of the Mo–S–H angle was studied, as shown in Fig. 7, keeping one SH group fixed. A high barrier of +36.4 kcal/mol at 117.0° and a low energy conformation, at 191°, were obtained. Note that all conformations are referenced to the conformation obtained after H_2 dissociation (starting conformation) with a Mo–S–H angle of 89°. Fig. 8a displays the starting, the highest and the lowest energy conformations, with the values of relative energies. The high barrier could be a consequence of the path chosen for opening the angle. A rotation by the Mo–S bond and then a change in the angle would lead to a lower barrier. Note that the angle opening was done keeping one Mo–S–H bond fixed; therefore, relaxing these bonds would diminish the barrier. Because the final state is about 57 kcal/mol more stable than the starting one, it is possible to transfer the second H atom to form a H_2S molecule adsorbed over the MoS_2 cluster. The proton transfer would go through a 3-center intermediate, as depicted in Fig. 8b. The final structure will lead to vacancy formation. A similar mechanism has been proposed by Massoth and Zeuthen [31], in order to explain the sulfur exchange process over MoS_2.

5. Conclusions

In this work we have studied for the first time the H_2 interaction with the sulphur atoms, from the topological point of view, on small clusters of MoS_2 (Mo_3S_6 and Mo_2S_6). Our results show that the maxima of $-\nabla^2\rho_{spin}(\boldsymbol{r})$ and not the maxima of $-\nabla^2\rho(\boldsymbol{r})$ gives the correct answer where the active sites are. According to ab initio ECP and $-\nabla^2\rho_{spin}(\boldsymbol{r})$ calculations, the H_2 is dissociated by a four-center mechanism that involves two neighbor S atoms and the H atoms of the H_2 molecule. The $-\nabla^2\rho_{spin}(\boldsymbol{r})$ topology shows that the S atoms have an unpaired charge concentration in such a spatial position (see Figs. 4 and 5) that the formation of a four-center intermediate is facilitated, and leads to H_2 bond breaking, and the formation of two –SH groups.

The three-center mechanism that involves one S atom and the H_2 molecule is difficult to verify at this theoretical level, because it seems to be necessary to include the electronic correlation that is absent at HF level. One may conclude, however, that the three-center mechanism would not lead immediately to the formation of H_2S, because two S–H bonds are formed and the H–H is broken, leading to the scission of the Mo–S bond. This situation is less favorable than in the four-center mechanism, because no Mo–S bond is broken in the latter. Once the H_2 is dissociated, one H atom may be stabilized as depicted in Fig. 8a. Then, a proton transfer could occur (Fig. 8b), forming H_2S absorbed over MoS_2 surface, which is rapidly desorbed, leading to a vacancy formation on the Mo atom.

Acknowledgements

The authors acknowledge the contribution of the Centro Científico IBM de Venezuela S.A. and the Centro de Investigaciones y Desarrollo de Petroleos de Venezuela (INTEVEP), for providing an IBM-RISC 6000 Model-530 workstation. They also thank Dr. Juan Rivero for helpful discussions, and Dr. Yosslen Aray for providing the EXTREM program.

References

[1] A.L. Dicks, R.L. Ensell, T.R. Phillips, A.K. Szczepura, M. Thorley, A. Williams and R.D. Wragg, J. Catal., 72 (1981) 266.

[2] (a) J.M.J.G. Lipsch and G.C.A. Schuit, J. Catal., 15 (1969) 179. (b) H. Kwart, G.C.A. Schuit and B.C. Gates, J. Catal., 61 (1980) 128. (c) J. Barbour and K. Campbell, J. Chem. Soc., Chem. Commun., (1982) 1371.

[3] A. Wambeke, L. Jalowiecki, S. Kasztelan, J. Grimblot and J.P. Bonnelle, J. Catal., 109 (1988) 320. (b) M. Vrinat, M. Breysse, C. Geantet, J. Ramirez, F. Massoth, Catal. Lett., 26 (1994) 25. (c) B. Delmon and J.L. Dallons, Bull. Soc. Belg., 97 (1988) 473.

[4] (a) E. Diemann, Th. Weber and A. Müller, J. Catal., 148 (1994) 288. (b) T.F. Hayden and J.A. Dumesic, J. Catal., 103 (1987) 366.
[5] A.B. Anderson, Z.Y. Al-Saigh and W.K. Hall, J. Phys. Chem., 90 (1988) 803.
[6] R. Pis Diez and A.H. Jubert, J. Mol. Struct. (Theochem), 210 (1990) 329.
[7] R. Pis Diez and A.H. Jubert, J. Mol. Catal., 73 (1992) 65.
[8] M. Neurock and R.A. van Santen, J. Am. Chem. Soc., 116 (1994) 4427.
[9] R.F.W. Bader and H. Essen, J. Chem. Phys., 80 (1984) 1943.
[10] R.F.W. Bader, P.J. MacDougall and C.D.H. Lau, J. Am. Chem. Soc., 106 (1984) 1594.
[11] R.F.W. Bader, Chem. Rev., 91 (1991) 893.
[12] R.F.W. Bader, Atoms in Molecules: a Quantum Theory., Clarendon Press, Oxford, 1990.
[13] J. Cioslowski, P.J. Hay and J.P. Ritchie, J. Phys. Chem., 94 (1990) 148.
[14] (a) A. Sierraalta and F. Ruette, J. Comp. Chem., 15 (1994) 313. (b) A. Sierraalta and F. Ruette, Int. J. Quant. Chem., (accepted).
[15] R.F.W. Bader, R.J. Gillespie and P.J. MacDougall, J. Am. Chem. Soc., 110 7329 (1988).
[16] R.J. Gillespie, Can. J. Chem., 70 (1992) 742.
[17] R.F.W. Bader, Molecules in Physics, Chemistry and Biology., Vol. III, 73, Kluwer, Dordrecht, 1989.
[18] R.F.W. Bader, P.L.A. Popelier, C.J. Chang, J. Mol. Struct. (Theochem), 255 (1992) 145.
[19] P.J. MacDougall, M.B. Hall, R.F.W. Bader and J.R. Cheeseman, Can. J. Chem., 67 (1989) 1842.
[20] V. Jonas, G. Frenking and M.T. Reetz, J. Comp. Chem., 13 (1992) 919.
[21] A. Veldkamp and G. Frenking, J. Comp. Chem., 13 (1992) 1184.
[22] MOTECC-90™, IBM Corporation Center for Scientific and Engineering Computation, Kingston, NY, 1990.
[23] R.G. Dickinson and L. Pauling, J. Am. Chem. Soc., 45 (1923) 1466.
[24] (a) M. Rakowski DuBois, Chem. Rev., 89 (1989) 1. (b) A. Müller, Polyhedron, 5 (1986) 323.
[25] W. Stevens, H. Basch and M. Krauss, J. Chem. Phys., 81 (1984) 6026.
[26] L.A. LaJohn, P.A. Christiansen, R.B. Ross, T. Atashroo and W.C. Ermler, J. Chem. Phys., 87 (1987) 2812.
[27] F.W. Biegler-Konig, R.F.W. Bader and T.H. Tang, J. Comp. Chem., 3 (1982) 317.
[28] R.W. Bader, T.H. Tang, Y. Tal and F.W. Biegler-Konig, J. Am. Chem. Soc., 104 (1982) 946.
[29] J. Polz, H. Zeilinger, B. Müller and E Knözinger, J. Catal., 120 (1989) 22.
[30] J. Yu and A.B. Anderson, J. Mol. Catal., 62 (1990) 223.
[31] F.E. Massoth and P. Zeuthen, J. Catal., 145 (1994) 216.